Published in final edited form as:
*Sci Transl Med*. 2011 May 25; 3(84): 84ra45. doi:10.1126/scitranslmed.3001577.

# Indocyanine Green Enables Near-Infrared Fluorescence Imaging of Lipid-Rich, Inflamed Atherosclerotic Plaques

**Claudio Vinegoni**[1,3], **Ion Botnaru**[2], **Elena Aikawa**[3,4], **Marcella A. Calfon**[2], **Yoshiko Iwamoto**[1], **Eduardo J. Folco**[4], **Vasilis Ntziachristos**[5], **Ralph Weissleder**[1,3], **Peter Libby**[4], and **Farouc A. Jaffer**[2,3,*]

[1]Center for Systems Biology, Massachusetts General Hospital, Boston, MA 02114

[2]Cardiovascular Research Center and Cardiology Division, Massachusetts General Hospital, Boston, MA 02114

[3]Center for Molecular Imaging Research, Massachusetts General Hospital, Boston, MA 02114

[4]Cardiovascular Division, Brigham and Women's Hospital, Boston, MA 02114

[5]Institute for Biological and Medical Imaging (IBMI), Helmholtz Center Munich & Technical University of Munich, Germany

## Abstract

New high-resolution molecular and structural imaging strategies are needed to visualize high-risk plaques that are likely to cause acute myocardial infarction, because current diagnostic methods do not reliably identify at-risk subjects. While molecular imaging agents are available for lower-resolution detection of atherosclerosis in large arteries, a lack of imaging agents coupled to high-resolution modalities has limited molecular imaging of atherosclerosis in the smaller coronary arteries [AU: ok? YES]. Here, we have demonstrated that indocyanine green (ICG), an FDA-approved near-infrared fluorescence (NIRF) emitting compound, targets atheromas within 20 minutes of injection and provides sufficient signal enhancement for in vivo detection of lipid-rich, inflamed, coronary-sized plaques in atherosclerotic rabbits. In vivo NIRF sensing was achieved with an intravascular wire in the aortae, a vessel of comparable caliber to human coronary arteries. Ex vivo fluorescence reflectance imaging studies showed high plaque target-to-background ratios in atheroma-bearing rabbits injected with ICG, compared to atheroma-bearing rabbits injected with saline. In vitro studies using human macrophages established that ICG preferentially targets lipid-loaded macrophages. In an early clinical study of human atheroma specimens from four patients, we found that ICG colocalized with plaque macrophages and lipids. The atheroma-targeting capability of ICG has the potential to accelerate the clinical development of NIRF molecular imaging of high-risk plaques in humans.

## INTRODUCTION

Rupture of atherosclerotic plaques and its associated thrombotic complications of myocardial infarction, stroke, and ischemic limbs remain leading causes of morbidity and

*Correspondence: Farouc Jaffer MD PhD, MGH Cardiovascular Research Center, Simches Research Building, 185 Cambridge Street, Room 3206, Boston, MA 02114, T: 617-724-9353, F: 617-643-3451, fjaffer@mgh.harvard.edu.

**LIST OF SUPPLEMENTARY MATERIAL**

Methods

Fig. S1. Experimental intravascular NIRF sensing protocol for ICG targeting of atheroma.

Fig. S2. Experimental setup for NIRF spectroscopic sensing.

Fig. S3. Histological sections and fluorescence images of human carotid endarterectomy specimens incubated with ICG.

mortality worldwide. Although various invasive and noninvasive imaging techniques can interrogate structural and compositional aspects of atheroma, only recently have molecular imaging strategies, such as nanoparticle-enhanced MRI and fluorine-18-fluorodeoxyglucose positron emission tomography, enabled the *in vivo* detection of high-risk plaque features, such as inflammation, in patients (1, 2). However while molecular imaging of larger arterial beds, such as the aorta, carotid, and iliac arteries, has experienced rapid clinical translation, high-resolution molecular imaging studies of smaller coronary arterial plaques remain scarce. Two main features contribute to this shortfall: (i) the requirement for high spatiotemporal resolution to image small-volume coronary atheroma, which can be less than 0.1 mL (3) and which typically necessitates intravascular imaging approaches (4); and (ii) the lack of sensitive molecular imaging agents that can be coupled to high-resolution detection modalities.

To address the first limitation, we recently developed high-resolution near-infrared fluorescence (NIRF) molecular imaging technology to sense protease activity in atheroma (5). This approach validated a clinical-type coronary artery guidewire for sensing intravascular NIRF signals at high resolution, and capitalized on the favorable optical properties of the near-infrared (NIR) window, namely relatively limited photon absorption by blood and reduced tissue autofluorescence (6, 7). Although the intravascular NIRF guidewire addressed a device-based need for high-resolution coronary arterial molecular imaging, the lack of a clinical NIRF molecular imaging agent has remained a barrier to translation. We therefore reviewed potential clinical candidate agents, and recognized that indocyanine green (ICG, $C_{43}H_{47}N_2O_6S_2Na$, molecular weight 775 Da), an amphiphilic NIR fluorochrome, appeared promising for molecular imaging of atherosclerosis in the clinic. ICG is a clinical cardiac and hepatic blood flow reporter that has been used for over five decades (8, 9), and is approved by the Food and Drug Administration for NIRF imaging of retinal and choroidal vasculature since the 1970s (10–12). ICG is composed of two lipophilic polycyclic moieties (benzoindotricarbocyanin) linked by a polymethine chain. A sulfonate group is bound to each polycyclic part, enhancing water solubility and conferring amphiphilic properties. As a result, after injection, ICG binds rapidly to plasma proteins, primarily albumin. Its absorption maximum is 785 nm in aqueous solution, and red shifts to 805 nm in blood; whereas its fluorescence emission maximum is 815 nm in aqueous solution, shifting to 830 nm in blood. After injection, ICG is rapidly taken up by the liver and then excreted, unchanged, into the bile, with an elimination half-life of 2 to 4 minutes in subjects with normal liver function (10).

Importantly ICG may detect certain molecular and cellular targets relevant to atherosclerosis; for example ICG binds low density lipoprotein (LDL) and high density lipoprotein (HDL), consistent with its lipophilic properties (13). Moreover, ICG can illuminate local inflammation in diseases of the eye (10, 14) and of the joints (15). On the basis of its high-resolution NIRF imaging capabilities, its lipophilic properties, and its predilection to accumulate at sites of inflammation, we hypothesized that ICG would enable in vivo detection of lipid-rich, inflamed atheroma and sought to test this hypothesis in a rabbit model of atherosclerosis. We also examined the ability of ICG to target human macrophages and human atherosclerosis specimens ex vivo.

## RESULTS

### ICG rapidly targets atherosclerosis on ex vivo NIRF imaging

To explore whether ICG could rapidly target experimental atherosclerosis, we generated lipid-rich, inflammatory atheroma in cholesterol-fed New Zealand white rabbits (n=19 total) (16, 17) with balloon injury of the aorta. Eight weeks after balloon injury, rabbits received an injection of ICG (n=17) at 1.5 mg/kg intravenous bolus, which is an FDA-approved dose

for clinical ICG applications (18), or saline (n=2). An additional two normal rabbits (chow diet, not balloon injured) were also injected with ICG (1.5 mg/kg) and served as controls. Forty-five minutes after ICG or saline injection, rabbits were sacrificed and imaged with fluorescence reflectance imaging. The plaque signal-to-noise ratio (SNR) and the plaque target-to-background ratio (TBR) were calculated for the acquired NIRF images. In atheroma-bearing animals injected with ICG, we used ex vivo macroscopic fluorescence reflectance imaging to note a strong focal NIRF signal in the abdominal aorta and iliac arteries (Fig. 1A). These areas colocalized with atherosclerotic plaques, as detected by white-light images. The vessel SNR was 13.9±7.5 in this group. Control animals exhibited very low (170–630% reduced) NIRF signals (Fig. 1B, C), with a vessel SNR of 1.9±0.1 in the atheroma/saline-injected group and 5.2±0.1 in the normal/ICG-injected group ($p<0.05$) (Fig. 1D). In rabbits with atheroma, the peak plaque TBR in the ICG-injected group was over 110% higher than in the saline group (3.4±1.1 versus 1.6±0.2; $p<0.05$) [OK?] (Fig. 1E).

### ICG colocalizes with lipid-rich and macrophage-rich atheroma

Fluorescence microscopy and histological analysis revealed that ICG plaque fluorescence colocalized with neutral lipid (e.g. triglyceride)-rich areas in rabbit atheroma, as visualized by Oil red O (ORO) staining (Fig. 2A, B). Areas of intense ORO and ICG staining were noted deep within the intimal plaque and often near the border with the external elastic lamina (Fig. 2A.1; Fig. 2B) [oK? Removed 1–3 of B, because they are all representing same concept.]. The ICG signal appeared strongest in ORO-stained zones with dense areas of lipid, rather than the smaller, punctate ORO-positive zones. ICG also colocalized with a subset of RAM-11–positive plaque macrophages, particularly lipid-associated foam cells, as evidenced by ORO staining (Fig. 2A.2; Fig. 2B). In rabbits, the association of ICG with other plaque macrophages appeared less robust, as some RAM-11–positive areas did not reveal ICG fluorescence (Fig. 2A.2; Fig. 2B). ICG also deposited far less in intimal areas containing smooth muscle cells (Fig. 2A.3), endothelial cells (Fig. 2A.4), collagen (Fig. 2A. 5), or elastin (Fig. 2A.6).

### ICG generates plaque NIR fluorescence and is distinct from autofluorescence

Multichannel fluorescence microscopy was used to assess the specificity of ICG for plaque targeting. ICG fluorescence (845 nm) colocalized with ORO-positive areas (Fig. 3A, B); whereas autofluorescence signal (535 nm) emanated from elastin fibers in the tunica media (Fig. 3A–C). Atheroma sections from saline-injected rabbits demonstrated relatively little NIR fluorescence, but still showed 535-nm autofluorescence signals from the media (Fig. 3C).

### Comparison of the atheroma-targeting profile of ICG with a vascular permeability agent

We noted mild superficial ICG enhancement of the luminal border infrequently in some atheromatous areas (Fig. 3A, B) and occasionally even in ORO-negative areas, without evidence of atherosclerosis (Fig. 3B). Therefore, to examine whether heightened endothelial permeability from atherosclerosis and/or a hyperlipidemic milieu accounted for ICG deposition in arteries, Evans blue, a chemical agent that reveals vascular permeability, and ICG were co-injected into atheroma-bearing rabbits (n=3). Rabbits were then sacrificed 45 minutes later. Capitalizing on the known profile of Evans blue in atherosclerosis (19) and its fluorescence properties [excitation range 400–630 nm; maximum peak emission of 660 nm (20)], we performed multichannel fluorescence microscopy on atheroma that were resected from the animals. Imaging at 710 nm, we could see that Evans blue deposited homogeneously within the plaque, indicating impaired endothelial barrier function (19, 21) (Fig. 4A). In contrast, ICG localized in more restricted regions within the atherosclerotic intima (Fig. 4B)—as demonstrated above (Fig. 2, Fig .3).

### ICG binds acetylated LDL and albumin, and internalizes in human macrophages in vitro

To determine whether ICG directly binds lipid deposits, as suggested by our histological results, solutions of ICG alone (100 μM), human acetylated LDL (acLDL) alone (2 mg/ml), and a pre-incubated combination of ICG (100 μM) and human acLDL (2 mg/ml) were loaded onto size-exclusion resin columns. Compared to ICG and acLDL alone, pre-incubation of acLDL and ICG produced a greater peak absorption in fraction 2 (~200 μL; high molecular weight species), consistent with binding of ICG to acLDL (Fig. 5A). Notably, acLDL alone did not absorb at 750 nm, demonstrating that ICG was the source of the 750-nm signal in the acLDL–ICG group. There was also little signal from ICG alone within fraction 2, given the smaller size of ICG. At the later elution volumes of approximately 800 μL (lower molecular weight species), a signal was noted in the ICG alone group, but with smaller peak values than in fraction 2, presumably due to interactions of ICG with the hydrophobic resin.

Macrophages can ingest albumin, and ICG can bind to albumin (10); therefore, we performed a size-exclusion column study of ICG (100 μM), bovine serum albumin (BSA; 1mg/ml), and a preincubated combination of ICG and BSA. Similar to the ICG–acLDL results, the preincubated ICG–BSA combination generated a strong optical absorption in elution fraction 2 (high molecular weight) that was absent in the BSA alone group (Fig. 5B). This finding suggests that macrophage uptake of ICG in vivo might occur by phagocytosis of ICG-albumin complexes.

To investigate ICG uptake by macrophages, human monocyte–derived macrophages (a subset of which were preloaded with acLDL to form foam cells) were incubated with or without ICG (25 or 125 μM). Fluorescence microscopy (810 nm) of foam cells incubated with ICG revealed strong NIR fluorescence, in contrast to control foam cells that showed negligible NIR autofluorescence (Fig. 5C). Macrophages incubated for 1 hour with ICG demonstrated concentration-dependent, fluorescence at 790 nm. AcLDL-induced foam cells showed higher ICG uptake than macrophages (Fig. 5D), in a concentration-dependent manner (Fig. 5E).

### ICG enables rapid in vivo detection of lipid-rich inflamed plaques

To determine whether ICG could provide suitable signal-to-noise for in vivo detection of atherosclerosis, cholesterol-fed, balloon-injured rabbits (n=5) underwent intravascular sensing using a coronary artery guidewire modified to detect NIR fluorescence (Fig. S1; Fig. S2). Nonuniform pullback was a limitation of our prior in vivo spectroscopic study (5). As such, to allow uniform pullback in 4 of 5 rabbits, the back end of the fiber was attached to an automated mechanism with a pullback rate of 0.5 mm/s. Rabbits underwent both X-ray angiography (Fig. 6A) and intravascular ultrasound (IVUS) (Fig. 6B) to enable precise co-registration of NIRF signals with X-ray– and IVUS–defined atheroma (Fig. 6C). After the intravascular NIRF guidewire was placed, baseline NIRF automated pullbacks across aortic atheroma (before ICG injection) revealed minimal NIRF signal (as in Fig. 7B), consistent with low autofluorescence and low electronic noise. ICG was then injected, and serial, dynamic NIRF guidewire pullbacks performed under X-ray guidance. After 10–15 minutes to permit ICG washout from the blood pool, focal NIRF signal evolved and co-localized with atheroma that had been co-registered by X-ray angiography and IVUS images (Fig. 6). The ex vivo fluorescence reflectance image (FRI) (Fig. 6D) and fusion NIRF-white light (WL) image (Fig. 6E) demonstrated a strong NIRF signal in aortic and iliac plaques, corroborating the in vivo NIRF pullback data.

The in vivo peak plaque target-to-background ratio in ICG-injected animals (n=5) was 10.3±6.2 (Fig. 7A), which was significantly greater than the baseline plaque TBR prior to

injection (1.4±0.2; $p<0.05$). NIRF signal profiles before ICG injection showed minimal autofluorescence signal (Fig. 7B, lower left). Analysis of the signals obtained during the serial NIRF guidewire pullbacks revealed that the initial peak arterial signal correlated with saturating blood concentrations of ICG and decayed exponentially over time (Fig. 7B). Approximately 15–20 minutes after injection, however, the peak ICG signal in the vessel localized to atheroma, indicating selective, focal retention of ICG in the plaques. The plaque TBR remained stable during the guidewire sampling period of 20 minutes until sacrifice at 45 minutes (Fig. 7C), demonstrating that ICG provided durable NIRF plaque enhancement over this time period.

To examine the capability of ICG to target and enhance human atheroma, ICG was incubated for 1 hour with freshly resected human carotid endarterectomy specimens at 37 °C (n=4 patients). NIR fluorescence microscopy and correlative histological evaluation revealed that ICG colocalized with human plaque macrophages, as evidenced by a fluorescent overlap with CD68+ staining (Fig. S3). ICG also colocalized with lipid-rich (ORO-positive) areas, although visually less so than macrophages. ICG did not specifically target collagen in human atheroma, as shown by lack of overlap with Masson's trichrome staining of collagenous areas (Fig. S3), and as corroborated by the *in vivo* ICG atheroma results in rabbits (Fig. 2A). We also noted NIRF signal present at the borders of the specimen, which reflects an edge artifact (Fig. S3.4). As opposed to intravenous injection of ICG in the rabbit study, where ICG may access the plaque interior via penetrating vasa vasorum, ex vivo binding of ICG to plaque components is likely to be diffusion-limited, which results in greater ICG access to the plaque edges compared to the interior of the plaque.

## DISCUSSION

Methods are needed to detect coronary arterial plaques that are at risk for rupture. Clinically approved atherosclerosis-targeted contrast agents could enable high-resolution clinical molecular imaging of coronary arterial pathology. Here, we have demonstrated that ICG, an FDA-approved NIRF imaging agent, targets lipid-rich and macrophage-rich atheromas. At clinically acceptable injection doses (18), ICG enables rapid (<20 minutes) intravascular *in vivo* detection of lipid-rich, inflamed experimental atheroma in blood-filled arteries of rabbits, similar in caliber (2.5 to 3.5 mm diameter) to human coronary arteries.

Our histopathological studies of rabbit and human atherosclerosis and in vitro cellular and biochemical analyses have established that the ICG signal reflects several features implicated in atherosclerotic plaque destabilization (22), including lipid and macrophage accumulation and possibly endothelial dysfunction, as gauged by heightened vessel permeability (Figs. 2–4; Fig. S3). ICG is lipophilic (10) and can bind to several plasma lipoproteins, including the atherogenic lipoprotein LDL (13). As such, plaque areas, including foam cell–rich zones, associate closely with ICG deposition (Fig. 2A, B; Fig. 3; Fig. S3). In vitro studies demonstrated that ICG bound to acLDL and to BSA was internalized within human macrophages and foam cells, thus extending prior data (23) and shedding new light on mechanisms that might govern ICG accumulation in plaques.

ICG was occasionally deposited in the subendothelial zones of the aorta of cholesterol-fed animals, even when atherosclerosis was not detected by Oil red O staining (Fig. 3B). Arteries of cholesterol-fed rabbits develop endothelial dysfunction (24) and ICG enters the vessel wall in areas of injured endothelium (25); in this context, we found that, although ICG enters the arterial wall in areas of dysfunctional endothelium and perhaps binds to endothelial cells (26), the overall contribution of a permeable endothelium to ICG-signal–

enhancement in vivo appears minor, compared to the larger contributions of ICG bound to lipids and macrophages (Figs. 2–3; Fig. S3).

We also investigated whether intravascular NIRF technology could be used with ICG to identify lipid-rich, inflamed atheroma in vivo in rabbits, as these features demarcate high-risk plaques responsible for acute myocardial infarction (27). The NIRF guidewire enabled sensitive in vivo detection of ICG through blood, with serial pullbacks revealing focal NIRF signal in areas of atheroma, as determined by fiducial co-registered X-ray angiography and IVUS imaging (Fig. 6). The in vivo results provide insights into the kinetics of ICG targeting to atheroma: (i) ICG clears rapidly from the blood, consistent with its short blood half-life of 2–4 minutes after injection (10); (ii) within 5 blood half-lives of ICG elimination (~15–20 minutes), coronary artery–sized plaques become detectable in vivo; (iii) ICG provides durable plaque NIRF signal enhancement with relatively stable TBRs; (iv) detectable NIRF signal in atheroma can be obtained with approved clinical dosages of ICG [1.5 mg/kg bolus, which is below the maximum FDA-approved dose of 2 mg/kg (18), especially when allometric scaling is considered (28)]; and (v) ICG provides sufficient SNR for detection of enhanced plaques through blood, without the need for balloon occlusion or saline flushing, which attests to the favorable photonic transmission properties of the near-infrared window (6, 7).

We do note that our study has limitations. ICG was not directly investigated in coronary arteries, although the rabbit aorta has a caliber similar to human coronary arteries. Additional mechanistic studies are required to determine whether ICG binds specific lipid components of plaque, such as oxidized LDL, although detection of lipid- or macrophage-rich atheroma demarcates a high-risk plaque subtype (27). As demonstrated by correlative fluorescence microscopy and immunohistochemical analyses, not all macrophages exhibited an ICG signal. Further studies analyzing ICG uptake by macrophage subsets (29) could prove insightful, but few reagents have been validated for subtyping macrophages in rabbits. For intravascular NIRF detection, we utilized a one-dimensional spectroscopic sensing fiber that is blind to two-thirds of the vessel circumference (5) and is thus subject to sampling bias. New two-dimensional rotational NIRF imaging catheters might overcome this limitation (30), provided that sufficient sensitivity can be attained. In addition, we anticipate that integrated single, rather than separate, NIRF and structural imaging catheters (optical coherence tomography and IVUS) might enable exact co-registration of NIRF signals with plaques. Additional ICG dosing and timing studies will further optimize the achievable plaque TBR and determine the time duration of detectable ICG signal in plaques. Increased sensitivity could also be obtained by blood displacement via saline flushing, but was not required in this study.

Our findings demonstrate that the FDA-approved agent indocyanine green can provide rapid in vivo biological imaging readouts of lipid- and macrophage-rich plaques in rabbit arteries, through blood-filled vessels, and that ICG targets inflamed, lipid-rich human atheroma specimens ex vivo. The present results offer the possibility of accelerating clinical intracoronary NIRF molecular imaging of atherosclerosis. In addition to providing biological readouts of high-risk plaques, intracoronary detection of plaque ICG could allow examination of the mechanism and efficacy of atherosclerosis therapeutics that alter plaque lipid or macrophages (32), and might further elucidate the role of inflammation in provoking coronary stent thrombosis (33).

# MATERIALS AND METHODS

## Animal model and animal preparation

Lipid-rich inflammatory atherosclerosis was induced in New Zealand white rabbits (weight, 3–3.5 kg; Charles River Laboratories) by balloon injury of the abdominal aorta and bilateral iliac arteries in combination with an atherogenic diet (16, 17). One week before balloon injury, rabbits consumed a high-cholesterol diet (1% cholesterol and 5% peanut Oil, C-30293, Research Diets, Inc.). Rabbits were anesthetized with intramuscular ketamine (35 mg/kg) and xylazine (5 mg/kg) injection. Anesthesia was maintained by mask inhalation of isoflurane (1%–5% v/v) and supplementary oxygen. Arterial balloon injury was performed with a 3F Fogarty arterial embolectomy catheter (Edwards Lifesciences). The catheter was advanced in a 4F sheath (Cordis) into the artery through the right common carotid artery, the balloon inflated to tension (0.2–0.6 mL) and a total of 3 pullbacks were performed. The introducer was then removed, and the carotid artery was ligated. We employed X-ray guidance during the procedure (Siemens). Rabbits continued on a supplemental high-cholesterol diet for 8 more weeks.

We therefore investigated 19 atherosclerotic animals (17 injected with ICG, 2 injected with saline). ICG (Akorn) was injected at a dose of 1.5 mg/kg for in vivo studies. Of the 17 ICG-injected rabbits, 5 were used for in vivo studies, and 3 others were co-injected with Evans Blue (6 mL of 0.5% solution, Sigma) (34). We also used normal New Zealand white rabbits injected with ICG (1.5 mg/kg, n=2). The total number of rabbits used in the study was 21. Two normal rabbits (chow diet, not balloon-injured) served as additional controls. The Subcommittee on Research Animal Care at Massachusetts General Hospital approved this experimental protocol for all procedures.

## Fluorescence reflectance imaging

After the rabbits were euthanized, the arterial tree was perfused with saline and dissected, and connective tissue was removed carefully. The macroscopic fluorescence distribution of ICG in resected vessels was mapped with a commercial fluorescence reflectance imaging (FRI) system (for atherosclerotic rabbits, n=19, BonSAI system, Siemens); for normal rabbits, n=2, Small Animal Imaging System OV110, Olympus) equipped with an excitation bandpass filter of 716–756 nm and an emission bandpass filter of 780–820 nm (Omega Optical). White light (WL) and ICG fluorescence images were obtained with integration times of 100 ms and 15 seconds, respectively. Fusion images were created with Matlab software.

## Histology

After euthanasia and saline perfusion, arteries underwent immediate FRI and then were fixed in 4% paraformaldehyde for 24 hours. Aortic rings were embedded in optical cutting temperature compound (Sakura Finetek), frozen in chilled isopentane, and sectioned in 6-μm segments. We performed hematoxylin and eosin staining for overall plaque morphology; Oil red O (ORO; Sigma) staining to identify lipid-loaded macrophages; Masson's trichrome (Sigma) staining to detect collagen; and van Gieson (Sigma) to show elastin fibers. Adjacent sections were preincubated with 0.3% hydrogen peroxide to inhibit endogenous peroxidase activity and then incubated with primary antibodies: monoclonal mouse anti-human CD31 (clone JC70A; Dako) for endothelial cells; monoclonal mouse anti-human smooth muscle α-actin (clone1A4; Dako); and monoclonal mouse anti-rabbit RAM-11 for macrophages (NeoMarkers). After washing with PBS, species-appropriate biotinylated secondary antibodies were applied, followed by avidin-peroxidase complex (Vectastain ABC kit, Vector Laboratories). The reaction was visualized with a 3-amino-9-ethyl-carbazole substrate (DakoCytomation). Sections were counterstained with Harris hematoxylin solution

(Sigma) and mounted. Images were captured with a whole slide microscope scanner (Nanozoomer, Hamamatsu) and with an Eclipse 50i (Nikon) combined with a CCD camera (SPOT RT, Diagnostic Instruments).

### Fluorescence microscopy

Fluorescence microscopy was performed with an upright epifluorescence microscope (Eclipse 80i, Nikon) equipped with a cooled CCD camera (Cascade 512B, Photometrics) and an inverted fluorescence microscope (Eclipse TE2000, Nikon) equipped with a CCD camera (Spot Insight QE, Diagnostic Instruments). Images with the epifluorescence microscope were obtained with the following filters: ICG (excitation 775±25 nm, emission 845±27 nm, dichroic 810 LP); Evans blue (excitation 650±22 nm, emission 710±25 nm, dichroic 680 LP); autofluorescence (excitation 480±20 nm, emission 535±25 nm, dichroic 505 LP). ICG images with the inverted fluorescence microscope were acquired with the following filters: excitation 710±37 nm, emission 810±45 nm, dichroic 750 LP.

All images were then analyzed with IP Lab Spectrum software (Scanalytics). Distributions of the ICG fluorescence were determined from images obtained with variable exposure times and subsequently normalized for intensity after noise removal.

### In vitro binding of ICG to acetylated LDL

To determine the binding affinity of ICG to human acLDL, we utilized a size-exclusion resin column (Zeba Spin desalting columns, Pierce). Samples of 100 µl containing ICG alone (100 µM), human acLDL alone (2 mg/ml) and the pre-incubated (37 °C for 10 min) combination of ICG (100 µM) and acLDL (2 mg/ml) were loaded onto columns. For BSA binding experiments, samples of 100 µl containing ICG alone (100 µM), BSA alone (1 mg/ml) and pre-incubated (37 °C for 10 min) combination of ICG (50 µM) and BSA (1 mg/ml) were loaded onto similar size-exclusion columns. The columns were then spun at 14,000 rpm for 1 min, and serial elutions of 100 µl aliquots (1000 µL total) were collected using normal saline. Fractions were transferred to a 96-well plate and read by a spectrophotometer with optical density set at 750 nm (Spectramax Plus, Molecular Devices).

### In vitro uptake of ICG by human macrophages

Human peripheral blood monocytes were isolated from freshly prepared leukocyte concentrates by differential centrifugation in Ficoll-Hypaque gradients (35). Adherent monocytes differentiated into macrophages over 10 days in culture in RPMI medium containing 5% pooled human serum, L-glutamine, penicillin, and streptomycin (36). Macrophage conversion into foam cells was achieved by loading them with 50 µg/mL of acLDL (Biomedical Technologies) for 72 hours. Unloaded macrophages and acLDL-loaded macrophages were incubated with or without ICG (25 and 125 µM) for 60 min. Cells were washed >3 times with PBS and the NIR fluorescence (ex/em 730/790 nm) was measured with a Kodak Digital Science Image Station 4000MM PRO (Eastman Kodak Company, Molecular Imaging Systems). White light and ICG fluorescence images of the cells were then acquired with an inverted fluorescence microscope.

### In vivo NIRF guidewire sensing of ICG

The protocol used for the in vivo imaging acquisitions in atheroma-bearing rabbits (n=5) 8 weeks after balloon injury is illustrated in detail in the flowchart of Fig. S1.

### X-ray angiography

Aortoiliac X-ray angiography was performed with a manual injection of low-osmolar iodinated contrast agent (5 mL iopromide, Bayer Healthcare) to image the arterial branches

and to determine anatomical landmarks. A radiopaque marker present on the tip of the IVUS catheter combined with the external reference marks (3.8 cm nails) provided the necessary fiduciary points to co-register the NIRF imaging data.

### Intravascular ultrasound (IVUS)

IVUS imaging employed a 3.2-Fr monorail catheter with a 40-MHz single-element rotational transducer located proximal to its radiopaque tip and enclosed†in an acoustic housing (Boston Scientific). The monorail IVUS catheter was advanced distally into position over a 0.014-inch coronary guidewire. Anatomical landmarks such as the renal vessel branches and the aortoiliac bifurcation were used as reference points. Motorized IVUS pullbacks were performed at 0.5 mm/s. The ultrasound beam resolution was 50 micrometers in the axial direction and 100 to 200 μm in the lateral direction. In order to minimize arterial vasospasm, 200 μg of nitroglycerin was administered before intravascular imaging.

### Intravascular NIRF sensing apparatus

In vivo ICG data were acquired with a custom-built NIRF guidewire sensing apparatus (Fig. S2) (5). Excitation light from a continuous wave laser diode at 750 nm is filtered to remove any component present in the ICG fluorescence detection channel. Next, the excitation light is coupled into a 3 dB beam splitter and guided through a fiber for clinical optical coherence tomography (5). The guidewire has an outer diameter of 0.41 mm and houses a 62.5/125 μm multimode fiber 200 cm in length. The floppy distal tip of the catheter allows for the fiber to be gently directed through the blood vessels and contains a radiopaque marker for X-ray detection. A prism at the end of the catheter reflects the light at 90 degrees with respect to the catheter axis, focusing the excitation beam on a near diffraction-limited spot size of 40 μm at a working distance of 2 mm. The ICG fluorescence signal is collected in epifluorescence mode, through the same optical path used for excitation and guided to a photomultiplier tube (H5783–20, Hamamatsu). Signal is digitized with a 16-bit resolution acquisition card at 1 kHz rate. Data noise reduction and subtraction is performed with Matlab software (MathWorks). The laser power utilized was <2 mW as measured by a power meter at the catheter tip.

### In vivo spectroscopic sensing of ICG

Rabbits with aortic atherosclerosis (n=5) underwent intravascular sensing of ICG distribution in vivo. First, the NIRF guidewire was inserted through the carotid artery sheath and percutaneously advanced to the infrarenal aorta. In 4 of 5 animals automated NIRF guidewire pullbacks of 0.5 mm/s were made with the same motorized pullback apparatus as that used for the IVUS imaging system and allowed the fiber to be uniformly scanned axially within the artery. Pullbacks (automated or manual) were made prior to and then every 5 to 10 min after ICG injection for up to 45 min. Each pullback was initiated far away from the plaque position as determined by both IVUS and X-ray angioscopy while the ICG fluorescence signal was recorded by the photomultiplier and then digitized by a data acquisition card at 1 kHz. X-ray imaging, through the use of fiducial points and in combination with the NIRF guidewire's floppy metal tip, allowed for axial co-registration of both NIRF and IVUS datasets.

### Co-registration of NIRF and IVUS images

Care was taken to place fiducial markers (3.8-cm nails) on the rabbit in proximity of the aorta and within the X-ray field of view. The 2D distribution of the fiducial landmarks enabled co-registration of both the IVUS and the optical signal, due to the presence of a radiopaque tip on both the optical and IVUS catheters. Angiography was performed at the

time of the stent placement and provided concomitant visualization of the arterial branching. Using the fiduciary coordinates, the automated NIRF signal pullback data were matched to both the angiography images and the IVUS scans before image fusion (Matlab).

### Image analysis

Fluorescence reflectance imaging (FRI) data were analyzed with Matlab software. The vessel SNR ratio was obtained as the ratio of the signal calculated on the identified plaque region, divided by the noise of the image calculated on proximal areas outside the artery volume. For all analyses, we employed similar-sized regions-of-interest. In addition, we used the white light images to exclude areas with high reflectivity owing to bleedthrough-induced artifacts from the emission filters.

Raw FRI data were normalized to the background signal and the TBR was calculated. We subtracted the calculated background signal to remove camera noise and the optical bleedthrough of the reflected light. White light images served to identify atheroma in each aorta that were then thresholded to outline the arterial contour. Vessel areas with excess fat were excluded from TBR and SNR analyses to avoid artifacts due to autofluorescence. Measurements on two regions-of-interest of similar area and with a length of approximately one cm were performed, with one containing the maximum plaque fluorescence intensity and the other centered in an uninjured area. FRI measurements from two normal rabbits obtained from the BonSAI system were compared to the atherosclerotic FRI measurements by determining the camera noise and subtracting its contribution in order to calculate TBR and SNR respectively.

For in vivo NIRF data, NIRF pullbacks were analyzed from the ICG-injected atheroma bearing rabbits. All the recorded traces were low-pass filtered and the maximum intensity recorded in proximity of the plaque. The maximum signal intensity was always localized in areas of atheroma. The blood background signal was defined as the NIR fluorescence signal measured in the distal part of an uninjured artery. The TBR was then defined as the ratio of the maximum signal intensity to the blood background signal. The measurement errors of the maximum signal and the background signal of each pullback trace were defined as the standard deviation of the noise calculated on the background signal. Error bars on the ratio (TBR) were then determined using the error propagation formula [37].

### Statistical analysis

Data are presented as mean ± standard deviation. Unpaired and paired Student's *t* tests were used to assess statistical significance. The one-way ANOVA test followed by a post-hoc Tukey's test was also used for multiple comparisons. Values of $p<0.05$ were considered statistically significant.

## Supplementary Material

Refer to Web version on PubMed Central for supplementary material.

## REFERENCES AND NOTES

1. Sanz J, Fayad Z. Nature. 2008; 451:953–957. [PubMed: 18288186]
2. Jaffer FA, Libby P, Weissleder R. Circulation. 2007; 116:1052–1061. [PubMed: 17724271]
3. Virmani R, Burke AP, Kolodgie FD, Farb A. J Interv Cardiol. 2002; 15:439–446. [PubMed: 12476646]
4. MacNeill B, Lowe H, Takano M, Fuster V, Jang I. Arterioscler Thromb Vasc Biol. 2003; 23:1333–1342. [PubMed: 12805071]

5. Jaffer FA, Vinegoni C, John MC, Aikawa E, Gold HK, Finn AV, Ntziachristos V, Libby P, Weissleder R. Circulation. 2008; 118:1802–1809. [PubMed: 18852366]
6. Jaffer FA, Libby P, Weissleder R. Arterioscler Thromb Vasc Biol. 2009; 29:1017–1024. [PubMed: 19359659]
7. Calfon MA, Vinegoni C, Ntziachristos V, Jaffer FA. Journal of biomedical optics. 2010; 15 011107.
8. Fox I, Brooker L, Heseltine D, Essex H, Wood E. Proc Staff Meet Mayo Clin. 1957; 32:478–484. [PubMed: 13465828]
9. Caesar J, Shaldon S, Chiandussi L, Guevara L, Sherlock S. Clin Sci. 1961; 21:43–57. [PubMed: 13689739]
10. Desmettre T, Devoisselle JM, Mordon S. Surv Ophthalmol. 2000; 45:15–27. [PubMed: 10946079]
11. Flower RW. Optical Engineering. 1995; 34:727–736.
12. Benson RC, Kues HA. Physics in Medicine and Biology. 1978; 23:159–163. [PubMed: 635011]
13. Yoneya S, Saito T, Komatsu Y, Koyama I, Takahashi K, Duvoll-Young J. Invest Ophthalmol Vis Sci. 1998; 39:1286–1290. [PubMed: 9620093]
14. Herbort CP, Bodaghi B, Lehoang P. J Fr Ophtalmol. 2001; 24:423–447. [PubMed: 11351218]
15. Fischer T, Gemeinhardt I, Wagner S, Stieglitz DV, Schnorr J, Hermann K-GA, Ebert B, Petzelt D, Macdonald R, Licha K, Schirner M, Krenn V, Kamradt T, Taupitz M. Acad Radiol. 2006; 13:4–13. [PubMed: 16399028]
16. Galis ZS, Sukhova GK, Kranzhofer R, Clark S, Libby P. Proc Natl Acad Sci U S A. 1995; 92:402–406. [PubMed: 7831299]
17. Aikawa M, Rabkin E, Okada Y, Voglic SJ, Clinton SK, Brinckerhoff CE, Sukhova GK, Libby P. Circulation. 1998; 97:2433–2444. [PubMed: 9641696]
18. Akorn. Indocyanine green for injection, USP. 2008
19. van Nieuw Amerongen GP, Vermeer MA, Nègre-Aminou P, Lankelma J, Emeis JJ, van Hinsbergh VW. Circulation. 2000; 102:2803–2809. [PubMed: 11104736]
20. Hed J, Dahlgren C, Rundquist I. Histochemistry. 1983; 79:105–110. [PubMed: 6196326]
21. Stehbens WE. Atherosclerosis. 1978; 30:343–349. [PubMed: 708491]
22. Libby P. Nature. 2002; 420:868–874. [PubMed: 12490960]
23. Rhodes JM, Lind I. Immunology. 1968; 14:511–525. [PubMed: 4871348]
24. Verbeuren TJ, Jordaens FH, Zonnekeyn LL, Van Hove CE, Coene MC, Herman AG. Circ. Res. 1986; 58:552–564. [PubMed: 3486053]
25. Kim D-E, Schellingerhout D, Jaffer FA, Weissleder R, Tung C-H. J Cereb Blood Flow Metab. 2005; 25:226–233. [PubMed: 15678125]
26. Flower RW. Retina. 1994; 14:283–284. [PubMed: 7973128]
27. Naghavi M, Libby P, Falk E, Casscells SW, Litovsky S, Rumberger J, Badimon JJ, Stefanadis C, Moreno P, Pasterkamp G, Fayad Z, Stone PH, Waxman S, Raggi P, Madjid M, Zarrabi A, Burke A, Yuan C, Fitzgerald PJ, Siscovick DS, de Korte CL, Aikawa M, Juhani Airaksinen KE, Assmann G, Becker CR, Chesebro JH, Farb A, Galis ZS, Jackson C, Jang I-K, Koenig W, Lodder RA, March K, Demirovic J, Navab M, Priori SG, Rekhter MD, Bahr R, Grundy SM, Mehran R, Colombo A, Boerwinkle E, Ballantyne C, Insull W, Schwartz RS, Vogel R, Serruys PW, Hansson GK, Faxon DP, Kaul S, Drexler H, Greenland P, Muller JE, Virmani R, Ridker PM, Zipes DP, Shah PK, Willerson JT. Circulation. 2003; 108:1664–1672. [PubMed: 14530185]
28. Sharma V, McNeill JH. Br J Pharmacol. 2009; 157:907–921. [PubMed: 19508398]
29. Mantovani A, Garlanda C, Locati M. Arterioscler Thromb Vasc Biol. 2009; 29:1419–1423. [PubMed: 19696407]
30. Razansky RN, Rosenthal A, Mallas G, Razansky D, Jaffer FA, Ntziachristos V. Optics express. 2010; 18:11372–11381. [PubMed: 20588998]
31. Stamper D, Weissman NJ, Brezinski M. J Am Coll Cardiol. 2006; 47:C69–C79. [PubMed: 16631512]
32. Rader D, Daugherty A. Nature. 2008; 451:904–913. [PubMed: 18288179]
33. Lüscher TF, Steffel J, Eberli FR, Joner M, Nakazawa G, Tanner FC, Virmani R. Circulation. 2007; 115:1051–1058. [PubMed: 17325255]

34. Asahara T, Chen D, Tsurumi Y, Kearney M, Rossow S, Passeri J, Symes JF, Isner JM. Circulation. 1996; 94:3291–3302. [PubMed: 8989143]

35. Böyum A. Scand J Clin Lab Invest Suppl. 1968; 97:77–89. [PubMed: 4179068]

36. Isoda K, Folco E, Marwali MR, Ohsuzu F, Libby P. Atherosclerosis. 2008; 198:307–312. [PubMed: 18164016]

37. Taylor, JR. An introduction to Error Analysis. University Science Books; 1996.

38. **Acknowledgements:** We thank A. Mauskapf, J.L. Guerrero, and M.C. John for rabbit surgical studies; G. Mallas for assistance with intravascular NIRF signal detection; G. Sukhova for histology and staining of human carotid endarterectomy samples; and P. Fumene Feruglio and T. Quillard for assistance in image processing. **Funding:** NIH R01 HL108229 (F.A.J.), American Heart Association Scientist Development Grant #0830352N (F.A.J.), Howard Hughes Medical Institute Career Development Award (F.A.J.), Donald W. Reynolds Foundation (E.A., R.W., P.L., F.A.J.). C.V. acknowledges support from NIH RO1-EB006432, PO1-AI054904. **Author contributions:** F.A.J. conceived the study, assisted in data analysis, acquired experimental rabbit data, and supervised the project. C.V. and F.A.J. wrote the manuscript. C.V. generated the in vivo imaging measurements and analyzed the data. I.B. led the surgical procedures, performed the IVUS and angiography measurements, and analyzed the microscopy and FRI data. E.A. and Y.I. performed histopathological analyses. M.A.C. and E.J.F. performed and analyzed the in vitro ICG uptake and binding studies and contributed to writing the paper. P.L., R.W., and V.N. assisted with experimental design and contributed to writing the paper. **Competing interests:** F.J. has received a patent for ICG detection of atherosclerosis that has been assigned to Massachusetts General Hospital (F. Jaffer, Detection of atherosclerosis using Indocyanine green. United States Patent Application 20100092389)

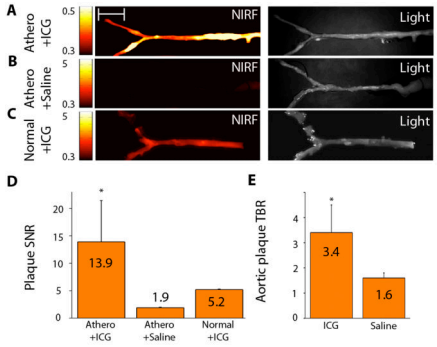


**Fig. 1.**

ICG rapidly targets atheroma in rabbit arteries and provides NIRF signal enhancement. Atheroma-bearing or normal rabbits were injected with either ICG or saline and then sacrificed after 45 minutes. (**A–C**) Ex vivo fluorescence reflectance images of aortas obtained at 800 nm (left column, fire color lookup table) and their corresponding white light images (right column). Scale bar, 2 cm. (A) A strong focal arterial NIRF signal colocalizes with atherosclerotic plaques seen in the white-light image of atheroma-bearing animals. (B) The saline-injected, atheroma-bearing group shows minimal NIRF arterial signal. (C) Normal, uninjured rabbits injected with ICG generate reduced, diffuse NIRF signal. All fluorescence images processed and windowed identically. (**D**) Signal-to-noise ratios (SNRs) were calculated for ICG-injected, atheroma-bearing animals (n=17); saline-injected, atheroma-bearing animals (n=2); and ICG-injected normal animals (n=2). The SNR in atheroma-bearing ICG injected animals was 170–630% higher than in control groups (*p<0.05, one-way ANOVA test across all 3 groups). (**E**) Plaque target-to-background ratios (TBRs) were 110% higher than the saline control group (*p<0.05, unpaired t-test). Data reported as mean +- standard deviation.

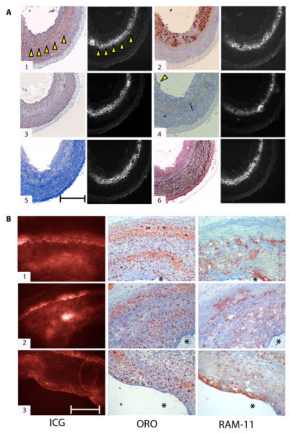


**Fig. 2.**

Histological assessment of ICG targeting of rabbit atheroma. (**A**) Correlative light microscopy and fluorescence microscopy of ICG deposition in atherosclerosis reveals ICG colocalization with lipid-rich and macrophage-abundant areas of atheroma sections. (1) Oil red O (ORO) stain of neutral lipid shows colocalization with ICG signal (arrowheads highlight the lipid-rich zone). (2) RAM-11–positive macrophages (dark brown stain) also colocalize with ICG, particularly in dense lipid-associated areas. (3) Immunoreactive smooth muscle cells (alpha-actin; stained brown) minimally colocalize with the matched ICG fluorescent area. (4) A few endothelial cells (CD31+) are present at the luminal surface (arrowhead). (5) Collagen (stained blue with Masson's trichrome) and (6) elastin fibers (stained black with von Gieson's) show very little colocalization with ICG. All histological slices are adjacent (6 μm). Fluorescence microscopic images of ICG distribution (854 nm) in all sections were obtained for each slice before staining. Scale bar, 200 μm. (**B**) Histopathological and fluorescence microscopic deposition of ICG in atheroma sections from three different animals. (1–3) From left to right: ICG fluorescence (845 nm, false-colored red), ORO staining of neutral lipid, and RAM-11+ macrophages. Within each group, all images are from adjacent sections (6 μm). Asterisk (*) denotes lumen. Scale bar, 100 μm.

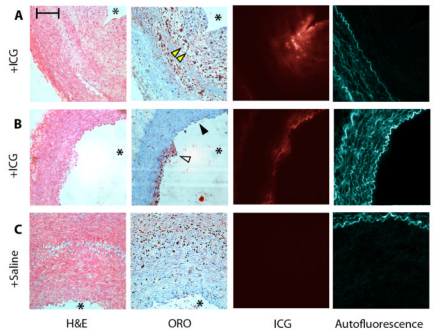


**Fig. 3.**

ICG deposition profile and autofluorescence in various-sized rabbit atheroma. From left to right: hematoxylin and eosin (H&E), for general morphology; Oil red O (ORO); 845 nm fluorescence channel for ICG (false-colored red); and 535 nm channel for autofluorescence from the medial elastic laminae (false-colored blue). Within each group, all images are from adjacent sections (6 μm) [OK?]. (**A**) ICG colocalizes with ORO-positive areas (arrowheads) in a larger atheroma section. (**B**) In a section from a small atheroma, ICG colocalizes with ORO (open arrowhead) and also generates a signal in the superficial intima-media in ORO-negative areas (solid arrowhead). (**C**) In saline-injected animals, minimal NIRF signal is evident, but 535 nm channel autofluorescence remains. Asterisk (*) denotes the location of the lumen. Scale bar, 100 μm.

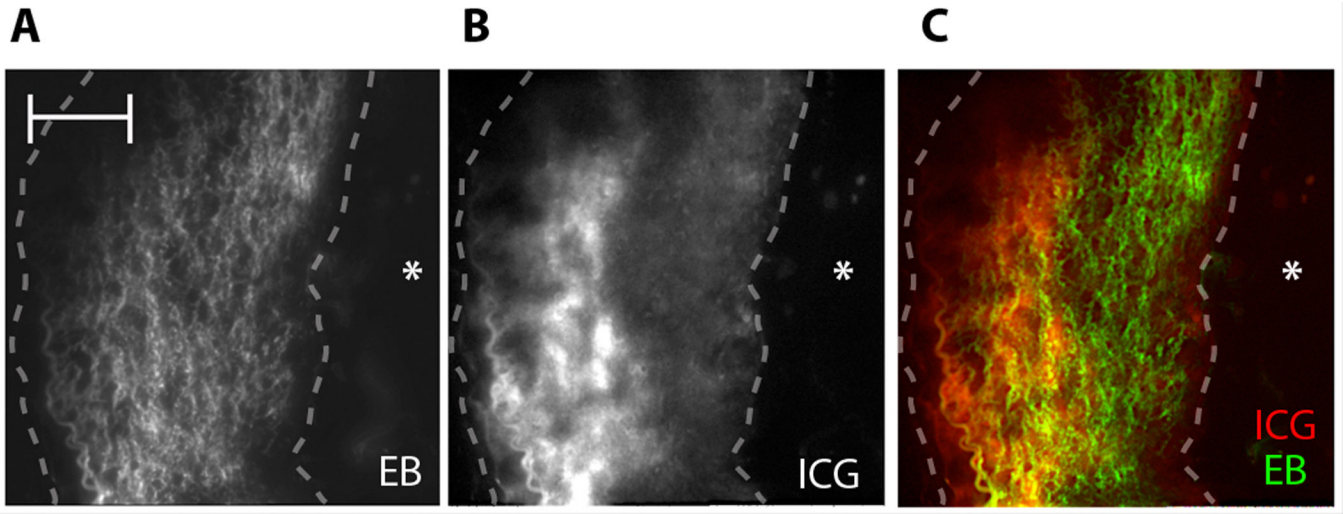


**Fig. 4.**

ICG atheroma-targeting profile in comparison to the Evans blue vascular permeability agent. (**A**) Fluorescence microscopy of Evans blue (EB) (710 nm) demonstrates homogenous signal enhancement in atheroma areas, indicating an impaired endothelial barrier. (**B**) ICG NIRF signal (845 nm) from the same section demonstrates focal signal in the deeper intimal plaque area. (**C**) A fusion image further illustrates the difference between ICG (red) and Evans blue (green) localization in an atheroma. Asterisk (*) denotes the location of the lumen. Dashed line outlines atheroma. Scale bar, 100 μm.

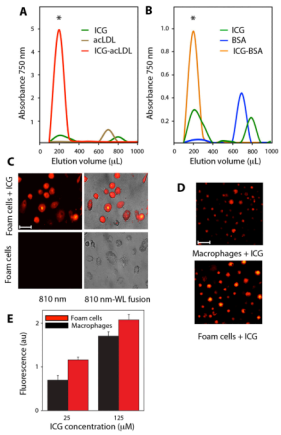


**Fig. 5.**

ICG binding to acetylated LDL (acLDL) and BSA, and uptake by human macrophages. (**A, B**) Size-exclusion chromatography with optical absorbance measured at 750 nm for serial elutions. Early elutions (*) consisted of higher molecular weight compounds. (A) Elution profiles of ICG, acLDL, and the pre-incubated ICG-acLDL combination. (B) Elution profiles of ICG, BSA, and the pre-incubated ICG-BSA combination. (**C**) Fluorescence microscopy of intracellular ICG uptake by foam cells (810 nm; fire color lookup table). Overlay of fluorescence with white light (WL) images is shown on right column. Scale bar, 50 µm. (**D**) ICG uptake by human macrophages and foam cells detected at 810 nm . Scale bar, 100 µm. (**E**) Fluorescence measurements (790 nm) of ICG (25 and 125 µM) uptake by human monocyte–derived macrophages and foam cells (average of n=2 experiments). Data reported as mean +- standard deviation.

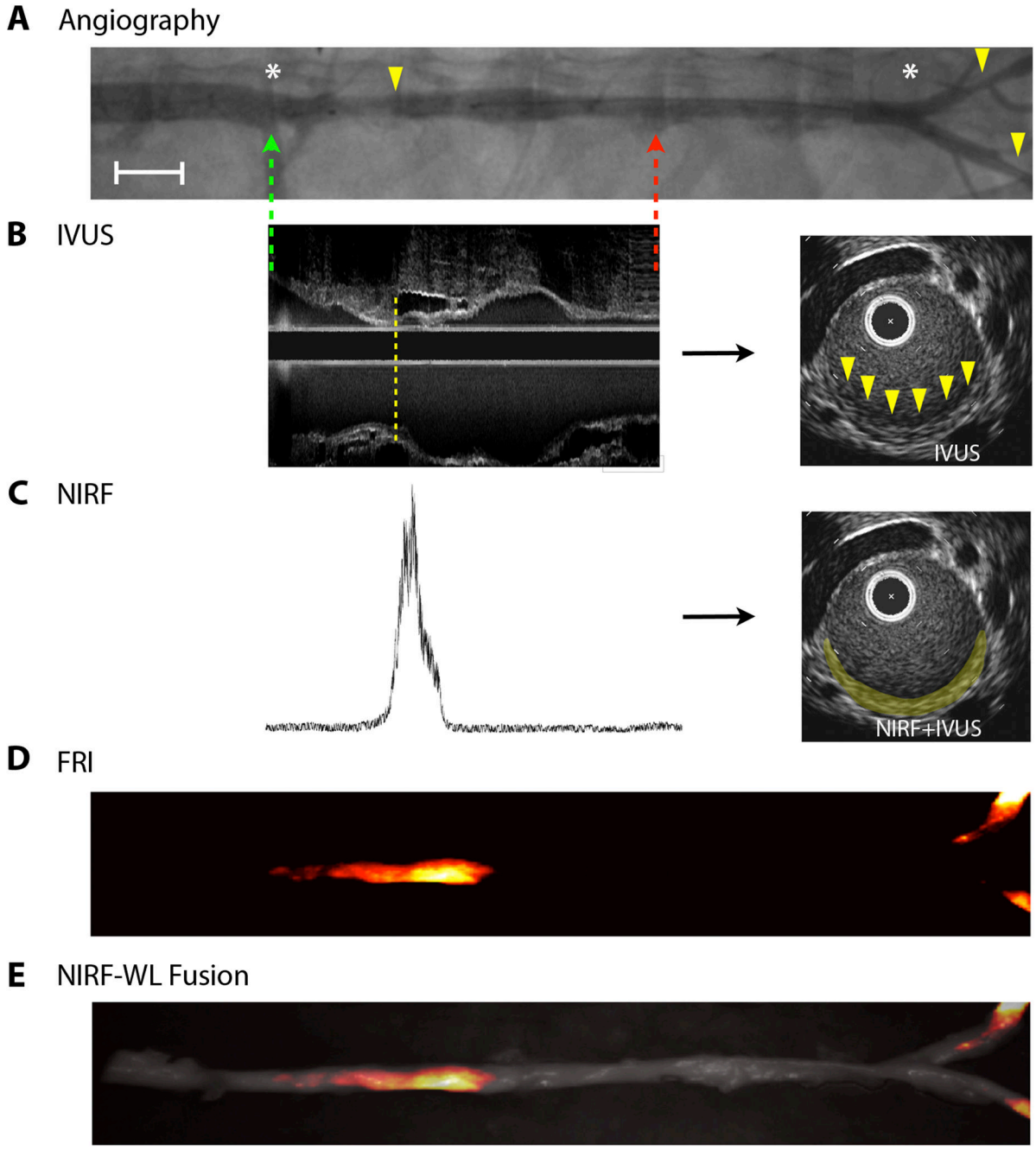


**Fig. 6.**

In vivo intravascular NIRF guidewire sensing of ICG localized in atherosclerotic plaques in rabbits. (**A**) X-ray angiographic images of aortic and iliac luminal narrowings (yellow arrowheads). Green and red dotted arrows represent the start and end of the NIRF guidewire pullbacks, respectively. The white asterisks demarcate arterial branch points. Image formed by merging two overlapping angiograms. Angiography, in combination with fiducial landmark coordinates from radiopaque tips on both the optical and IVUS catheters (not shown), allowed for co-registration of the NIRF and IVUS datasets. Scale bar, 1 cm. (**B**) IVUS longitudinal image obtained from an aortic atheroma-bearing animal (left). A small plaque (intimal thickening) is evident at the lower edge of the dotted yellow line, as seen

further on the corresponding axial image (right, yellow arrowheads). (**C**) Fifteen minutes after ICG injection, a NIRF guidewire signal trace was recorded at 780 nm during automated pullback (left). The NIRF signal (right, false-colored yellow) was fused onto the IVUS-demarcated atheroma in the axial slice shown in (B). All longitudinal images were scaled on the same unit length and matched on the same fiducial markers. (**D**) Ex vivo fluorescence reflectance images (FRI) show enhanced ICG signal in aortic and iliac plaques (fire color lookup table). (**E**) Overlay of FRI with the white light (WL) image.

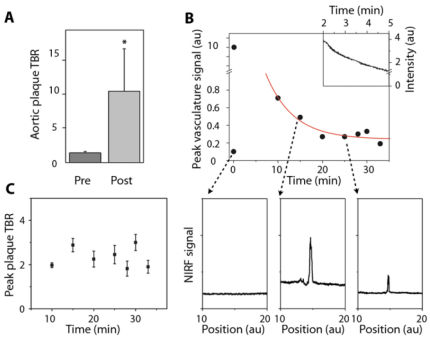


**Fig. 7.**

Focal ICG deposition in rabbit atheroma evolves rapidly after injection and provides stable target-to-background ratios (TBRs). After ICG injection, serial NIRF guidewire pullbacks were performed in vivo through blood, with each pullback initiated distal to plaques and with the starting position confirmed by both IVUS and X-ray angiography. (**A**) The maximum plaque TBR was 10.4±6.2 in the rabbits (n=5) studied. *$p<0.05$, paired t-test, versus the maximum pre–ICG-injection TBR. (**B**) Immediately after ICG injection, the NIRF guidewire signal recorded a saturating signal (10 au) owing to high concentration of ICG in the blood, followed by a rapid exponential decay (upper inset). A representative baseline NIRF signal during manual guidewire pullback, prior to ICG injection is shown (below, left). Fifteen minutes (below, middle) and 25 minutes (below, right) after ICG injection, the NIRF signal presented focal peaks at the site of the atheroma, as visualized on corresponding X-ray angiograms and registered in real-time during X-ray fluoroscopic tracking of the radiopaque NIRF guidewire. Each data point depicts one measurement. The red line shows a best fit with an exponential decay of the data points from 10 to 33 minutes. (**C**) Over the course of the imaging session (approximately 45 minutes), the ICG peak plaque TBR remained stable (n=5). Error bars show the measurement error of each TBR data point.